Environment-Dependent Radiation Damage in Atmospheric Pressure X-ray Spectroscopy

Robert S. Weatherup[1,2,*], Cheng Hao Wu[1], Carlos Escudero[3], Virginia Pérez-Dieste[3], Miquel B.

Salmeron[1,4]

[1]Materials Sciences Division, Lawrence Berkeley National Laboratory, 1 Cyclotron Road,

Berkeley, California 94720, United States

[2]Department of Chemistry, University of Cambridge, Lensfield Road, Cambridge CB2 1EW, UK

[3]ALBA Synchrotron Light Source, Carrer de la Llum 2–26, 08290 Cerdanyola del Vallès,

Barcelona, Spain

[4]Department of Materials Science and Engineering, University of California, Berkeley, United

States

ABSTRACT

Atmospheric pressure x-ray spectroscopy techniques based on soft x-ray excitation can provide powerful interface-sensitive chemical information about a solid surface immersed in a gas or liquid environment. However, x-ray illumination of such dense phases can lead to the generation of considerable quantities of radical species by radiolysis. Soft x-ray absorption measurements of Cu films in both air and aqueous alkali halide solutions reveal that this can cause significant evolution of the Cu oxidation state. In air and NaOH (0.1 M) solutions, the Cu is oxidized towards CuO, whilst the addition of small amounts of CH_3OH to the solution leads to reduction towards Cu_2O. For Ni films in $NaHCO_3$ solutions, the oxidation state of the surface is found to remain stable under x-ray illumination, and can be electrochemically cycled between a reduced and oxidized state. We provide a consistent explanation for this behavior based on the products of x-ray induced radiolysis in these different environments, and highlight a number of general approaches that can mitigate radiolysis effects when performing operando x-ray measurements.

INTRODUCTION

Many reactions of considerable economic and societal importance take place at the interfaces between different states of matter, from the conversion of the toxic products of combustion to less harmful emissions, to the reversible incorporation of ions at electrode-electrolyte interfaces in rechargeable batteries, along with many more examples from the fields of heterogeneous catalysis and electrochemical energy storage.[1–3] Probing and understanding the chemistry that occurs at such interfaces under realistic process conditions is crucial in the selection and design of improved materials for these applications. X-ray core-level spectroscopies can provide powerful element- and chemical-state-specific information, and there has thus been a concerted effort over the last decade to adapt these techniques to enable the operando characterization of solid-gas and solid-liquid interfaces under atmospheric pressure conditions.[4,5] In particular, interface-sensitive techniques based on soft x-ray excitation have been combined with impermeable membranes that seal an atmospheric pressure reaction cell, maintaining vacuum conditions in the measurement chamber whilst remaining largely transparent to x-rays, and in some cases the photoelectrons generated.[4,6–9]

The processes of photoionization and relaxation that underlie x-ray core-level spectroscopies, are commonly accompanied by radiolysis through ionic fragmentation and the interactions of secondary electrons.[10,11] In gas environments, as the pressure is increased the number of scattering events occurring within a given volume also increases, thereby increasing the amount of energy absorbed and the associated radical generation. This becomes even more pronounced when dealing with liquids, whose densities are typically three orders of magnitude greater than atmospheric pressure gases. Excitation with soft x-rays offers higher photoionization cross-sections of core electrons for x-ray photoelectron spectroscopy (XPS),[12] and nm-scale interface

sensitivity for XPS and total electron yield (TEY) mode x-ray absorption spectroscopy (XAS) due to the relatively low kinetic energies, and thus mean-free paths, of emitted photoelectrons. However, this also corresponds to dissipating significant energy close to the illuminated interface. Therefore under the conditions of atmospheric pressure x-ray spectroscopy significant radiolysis may occur close to the interface being probed. Although the effects of electron-beam irradiation have been widely discussed in relation to electron microscopy in dense liquid and gas environments,[13–17] as well as XPS at pressures of ~1 mbar,[18,19] reports that explicitly consider radiolysis effects in the context of atmospheric pressure x-ray spectroscopy remain scarce.[20] A more detailed understanding of these processes and how they influence the measurements being performed is thus needed as these techniques become more widely applied in material science research.

Here we use soft x-ray absorption spectroscopy in both TEY and total fluorescent yield (TFY) modes to study the oxidation state of Cu and Ni thin-film electrodes in air and aqueous solutions under electrochemical control. We find that Ni can be cycled between reducing and oxidizing conditions whilst simultaneously acquiring x-ray absorption spectra in TEY mode that reveal the corresponding oxidation state of the surface. For Cu we find that illumination with the x-ray beam already induces changes in the oxidation state of the Cu film. TEY mode is found to be most sensitive to this, with dramatic changes in oxidation observed between consecutive spectra whilst in TFY mode the spectra evolve more gradually, indicating that the observed changes originate at the solid-liquid interface rather than in the electrode bulk. Importantly, we reveal that the evolution of the Cu oxidation state during x-ray illumination depends critically on its environment. In air and aqueous alkali hydroxide solutions, Cu is found to gradually oxidize towards CuO over time. The addition of a small amount of methanol (CH_3OH) to the alkali

hydroxide solutions results in the reduction of the Cu film towards metallic Cu_2O. We rationalize these observations based on the radiolytic processes occurring in the gas or liquid environment close to the interface, where the radicals formed can react with the metal films. We discuss the relevance of these results to recent efforts to perform x-ray spectroscopy under ambient or atmospheric pressure conditions, and possible approaches that can be taken to mitigate such radiolysis effects.

EXPERIMENTAL METHODS

Figure 1 shows a schematic representation of the three-electrode electrochemical flow cell that allows in situ XAS measurements to be performed in both TEY and TFY modes (as indicated) which is similar to that previously described elsewhere.[6] The working electrodes consist of 50 nm thick Cu or Ni films deposited by electron beam evaporation ($<10^{-7}$ mbar base pressure) onto 100 nm thick Si_3N_4 membranes suspended across 500 μm thick silicon frames (1.0 × 0.5 or 1.0 × 1.0 mm window in a 10 × 10 mm frame). This is sealed against a viton o-ring to separate the inside of the cell, which contains either an aqueous solution or atmospheric pressure air, from the ultra-high vacuum conditions in the measurement chamber. The inside of the cell and the tubing that supplies it are made from polyether ether ketone (PEEK) whilst the surfaces on the vacuum side are constructed from stainless steel. A Pt wire is used as the counter electrode and a Ag wire as a pseudo-reference electrode. A Biologic MPG-2 potentiostat is used for electrochemical control. No flow is applied to the cell during spectrum acquisition, with a flow only used to change or refresh the environment within the cell between measurements.

TEY measurements are performed using the near-ambient pressure photoemission (NAPP) endstation at beamline 24 (CIRCE) of ALBA, the Barcelona synchrotron.[21] The x-ray beam is

chopped with a motorized rotating slotted disk, whose frequency is measured using an optical switch modulated by the same slotted disk, and controlled to maintain a designated frequency (20-1000 Hz). The current from the WE is amplified with a SR570 low-noise current amplifier (Stanford Research Systems) and then fed to a SR830 lock-in amplifier (Stanford Research Systems) where the modulated photocurrent is separated from any faradaic current, using the signal from the slotted optical switch as the frequency reference.[22] The chopper frequency is selected to maximise the signal to noise ratio of the measured x-ray absorption spectra. Spectra are normalized to the incident photon flux, measured via the current supplied to a Au mesh or the Au-coated refocussing mirror. For the Ni-$L_{2,3}$ edge measurements the photon flux reaching the sample is $\sim 2.3 \times 10^{12}$ photon/s and the spot size is $\sim 50 \times 100$ μm^2, whilst for the Cu-L_3 edge the photon flux is $\sim 4.1 \times 10^{12}$ photon/s and the spot size is $\sim 100 \times 100$ μm^2, as measured using a Si photodiode.

TFY measurements were acquired using a negatively biased channeltron at beamline 8.0.1 of the Advanced Light Source, the Berkeley synchrotron facility. Spectra are normalized to the incident photon flux, measured via the current supplied to a Au mesh. The photon flux reaching the sample is $\sim 2.5 \times 10^{12}$ photon/s and the spot size is $\sim 30 \times 150$ μm^2, as measured using a Si photodiode. The photon flux per unit area therefore remains similar across all of our measurements ($\sim 5 \times 10^8$ $\mu m^{-2} s^{-1}$), including both the TEY and TFY mode experiments as well as those at different absorption edges.

RESULTS AND DISCUSSION

Figure 1B shows a cyclic voltammogram (CV) for a Ni film (50 nm) cycled between -0.5 V and 0.6 V against a Ag pseudo-reference electrode in an aqueous solution of $NaHCO_3$(0.5 M). This solution has a pH of ~ 8.3, which according to the Pourbaix diagram for Ni should avoid any

significant dissolution of the electrode as Ni^{2+} ions.[23] Two distinct peaks at ~0.0 V and ~0.4 V, identified with vertical arrows, correspond to reduction and oxidation of the Ni surface respectively. Figure 1C shows the Ni $L_{2,3}$-edge measured in TEY mode before and during electrochemical cycling at the approximate voltages indicated with colored dots in Figure 1B. In air (black) before introducing the solution, the presence of a double peak in the L_2-edge region indicates that the surface is oxidized to Ni^{2+}.[24] This corresponds to the thin, passivating oxide/hydroxide layer that forms on the surface of metallic Ni when exposed to air, which protects against oxidation of the Ni bulk.[25–27] Following introduction of the $NaHCO_3$ solution (grey) and after biasing the working electrode to 0.1 V (red), the spectrum appears very similar indicating that the surface remains oxidized, consistent with the position on the acquired CV curve (Figure 1B). On cycling to -0.5 V (orange) the main peak of the Ni L_3-edge becomes more asymmetric and shifts to slightly lower photon energy, while the higher energy peak of the Ni L_2-edge disappears, indicating the reduction of the surface to metallic Ni.[24] As the electrode is cycled through -0.1 V (green), and 0.2 V (cyan) the Ni $L_{2,3}$-edge features remain similar, with an asymmetric main peak at the L_3-edge and a single peak at the L_2-edge, indicating the presence of predominantly metallic Ni. Previous studies report the formation of a layer of a nickel hydroxide at similar potentials,[28] but this is not apparent from our measurement of the Ni $L_{2,3}$-edge. However, we note that corresponding O K-edge spectra (see supporting information, Figure S1) show a small peak at ~531eV for all potentials measured except for -0.5 V, and this feature may relate to the presence of hydroxide at the surface. Only after cycling to a potential higher than the oxidation peak marked in Figure 1B, i.e. 0.5 V (blue), does the Ni $L_{2,3}$-edge spectrum change significantly indicating the surface is oxidized to Ni^{2+}, consistent with the formation of an oxide layer containing $Ni(OH)_2$, and possibly NiO.[28–33] We thereby confirm that we are able to collect

TEY spectra under electrochemical control using a three-electrode flow cell, and that changes in the oxidation of the Ni surface can be observed thanks to the inherent surface sensitivity (electron inelastic mean free path of ~1.3 nm in Ni at 850 eV[34]), even when only thin, self-limiting oxide/hydroxide layers are expected to form.[28,32,33]

Figures 2A, B show the evolution of Cu L_3-edge for Cu films (50 nm) measured with the cell filled with air (1 bar) using TEY and TFY modes respectively. The initial TEY spectrum (red) indicates that the surface consists of predominantly Cu_2O (main feature at ~933.5 eV) with a very small contribution from CuO (main feature at ~930.0 eV), indicative of oxidation of the surface during the ~1 week air exposure prior to measurement. With continuing x-ray illumination the proportion of CuO at the surface of the film increases with time (orange, green spectra) until it completely dominates (blue spectrum). The TFY measurements, although performed under similar conditions to the TEY measurements, used a sample that had been stored in air over a longer period (~6 months). In this case a more substantial CuO component is observed in the first scan, consistent with this longer air exposure, which grows in intensity with continuing x-ray illumination. In contrast to the TEY measurements, three resonances (~932.6, ~936.8, and ~941.0 eV) associated with metallic Cu are visible throughout the measurements. Considering the much longer attenuation length of the x-rays that contribute to the TFY signal (>50 nm for x-ray energies of 250-950 eV in Cu[35]), compared to that of the electrons that contribute to the TEY signal (inelastic mean free path of ~1.5 nm in Cu at 930 eV[34]), these results indicate that the Cu surface in contact with the air is rapidly oxidized towards CuO during x-ray illumination while the initially metallic Cu bulk, oxidizes progressively from the surface inwards. This accelerated oxidation behavior in air, over the course of 1-2 hours, is attributable to reactive oxygen species (ROS) produced by the radiolysis of air close to the Cu surface.[36] We

have previously observed similar behavior for Cu nanoparticles at room temperature using atmospheric pressure x-ray photoelectron spectroscopy (XPS), where under x-ray illumination the Cu oxidized towards CuO in the presence of O_2(1 bar) whilst it was reduced back toward Cu_2O/Cu under vacuum conditions.[9]

Figure 2C shows that this oxidation continues even as the environment is changed to an aqueous solution of NaOH(0.1 M). This corresponds to a pH of 13.0 and thus, according to the Pourbaix diagram for copper,[23] there should not be significant dissolution of the electrode as Cu^{2+} ions. The CuO peak seen in the TFY spectra continues to increase in intensity with continuing x-ray illumination and eventually CuO dominates (See red spectrum in Figure 3B) indicating the Cu film has been oxidized throughout its thickness. In this case, ROS created by the radiolysis of water[13,16] are expected to be responsible for the continuing Cu oxidation, although there may also be some contribution from air dissolved in the solution, which was not degassed prior to measurement. We note that water radiolysis is well-documented under both focused x-ray[7,18,20] and electron beams[4,13–17] and the resulting oxidative attack of graphene membranes has also recently been reported.[4,15]

Figure 3 shows the effect of adding a small amount (~0.1 M) of CH_3OH to 0.1 M aqueous solutions of alkali hydroxides (NaOH/KOH, pH of 13.0), where the Cu has previously been oxidized either electrochemically (TEY measurements) or by extended exposure to the x-ray beam under the conditions of Figure 2B,C (TFY measurements). At the first position measured (point A, Figure 3A) in TEY mode, the initial spectrum (red) shows features of both CuO and Cu_2O. In the next spectrum (orange) measured after a further 300s of x-ray illumination, the CuO component is completely absent and a peak at ~937.0 eV emerges, consistent with the second resonance of metallic Cu, indicating the reduction of the surface. Although the most

intense features of Cu_2O and metallic Cu overlap in energy, in comparison to purely metallic Cu the second resonance peak here is weaker with respect to the first resonance peak,[37,38] indicating a mixed Cu^+/Cu^0 oxidation state. This significant change between consecutive spectra suggests that considerable changes in Cu oxidation state occur during each measurement, and for this reason the scan range in Figure 3A is kept narrower than for Figure 2 to minimize measurement time. Moving to a new position (point B, Figure 3A) the first TEY spectrum (cyan) again indicates the presence of CuO and Cu_2O, consistent with regions of the Cu surface away from the x-ray beam remaining oxidized and thus further confirming that the reduction observed at point A was induced by x-ray illumination. The slightly lower CuO contribution is likely to be associated with a slightly longer x-ray illumination whilst aligning the beam on this point prior to measurement. Again with continuing x-ray illumination the subsequent TEY spectrum (blue) shows dramatic changes, with the removal of the CuO feature indicating reduction of the Cu surface. No peak is discernable at the position of the second resonance of metallic Cu indicating that the surface is now predominantly Cu_2O. This lesser state of reduction is consistent with the shorter x-ray illumination time because, unlike point A, there was no significant x-ray exposure between the measurement of the first and second spectrum.

The TFY spectra of Figure 3B show that in this experiment the Cu film initially consists of exclusively CuO throughout its thickness, as indicated by a single strong component at ~930.0 eV (red spectrum). The intensity of this CuO peak then gradually reduces in intensity to leave predominantly Cu_2O (green spectrum) and then eventually the second resonance of metallic Cu emerges (violet spectrum). This evolution of the Cu oxidation state is qualitatively similar to the reduction of the Cu film that is seen in TEY mode but appears to proceed over a longer timescale, despite the photon flux per unit area being similar for both measurement modes.

Considering that the TEY signal is much more surface sensitive, this behavior therefore indicates that the Cu surface is rapidly reduced and that reduction of the rest of the Cu film then proceeds inwards from this surface. Indeed, given the significant changes seen between consecutive TEY spectra, it is reasonable to assume that the whole film is initially CuO, but the surface is already starting to be reduced by the time the energy range where the Cu_2O peak is swept (i.e. after ~90 s of x-ray illumination). The fact that this reaction proceeds from the solid-liquid interface, again indicates that radiolysis of the liquid environment is responsible for the change in oxidation state of the Cu electrode. However, the shift from oxidation to reduction of the Cu electrode simply by adding a small amount of CH_3OH to the liquid environment indicates that radiolysis of this solution is now yielding an increased proportion of reducing species, changing the balance towards reduction of the Cu surface.

Our results clearly highlight that the radiolysis induced by x-ray illumination can significantly influence the observed behavior when performing atmospheric pressure x-ray spectroscopies, and must therefore be carefully considered. Most significantly we observe that the impact of this radiolysis is highly dependent on the electrode material and the environment in which it is placed. We note that throughout our measurements the x-ray flux per unit area is very similar (see methods) and thus variations in illumination are not responsible for the observed differences in behavior. To understand the origin of these differences we first consider the x-ray illumination of the Cu and Ni electrodes in atmospheric air, where air radiolysis is expected to produce ozone (O_3) as its major product.[36] For Cu (Figures 2A,B), the evolution from a predominantly Cu^+ oxidation state towards predominantly Cu^{2+} is attributable to the strong oxidizing effect of the ozone generated. For Ni (Figure 1 C), we observe that although the oxidation state of the surface is Ni^{2+} from the start of measurement there is no significant evolution during repeated

measurements in air over the course of several hours prior to introducing the $NaHCO_3$ solution, with no detected increase in Ni^{3+} contribution.[39–41] This is consistent with a thin oxide/hydroxide layer having already formed on the Ni surface during prior air exposure,[25,27,42] which passivates against further oxidation even in the presence of ozone generated by radiolysis of the surrounding air.

When measuring in liquid environments, such as the aqueous solutions used herein, the effects of radiolysis may be even more severe given the higher density of liquid phases. The major oxidizing products of water radiolysis are O_2, H_2O_2, and $^{\bullet}OH$.[13,16,43–46] A relatively high concentration of $^{\bullet}OH$ is expected to develop in spite of its high reactivity, due to its large primary radiation yield and the scarcity of reactive species in water with which it can annihilate.[13] Given that the standard electrode potentials for molecular oxygen, $E^0(O_2/H_2O) = 1.23$ V,[47,48] hydrogen peroxide, $E^0(H_2O_2/H_2O) = 1.77$ V,[47,48] and hydroxyl radicals, $E^0(^{\bullet}OH/H_2O) = 2.73$ V,[49,50] are significantly higher than those for copper oxidation, $E^0(Cu_2O/Cu, H_2O) = 0.471$ V[23] and $E^0(CuO/Cu_2O, H_2O) = 0.669$ V,[23] these species are primarily implicated in the Cu film oxidation observed during x-ray illumination in the NaOH(0.1 M) solution (Figure 2C). We note that all of the electrode potentials considered here should be adjusted by -0.0592 V/pH as the pH is varied and thus the relative differences between them remain unchanged irrespective of the solution's pH.

For the Ni electrodes, such beam-induced oxidation is not detected during measurement, with significant changes in the Ni $L_{2,3}$-edge only seen after passing through potentials corresponding with the oxidation and reduction peaks of the CV curves obtained without illumination. This therefore confirms that the oxidation state of the Ni electrode remains as expected throughout the electrochemical cycling. In contrast to the Cu measurements, an aqueous $NaHCO_3$ electrolyte is

12

used here, and we therefore suggest that the electrode's stability may be related to the presence of bicarbonate anions which are known to scavenge hydroxyl species that may otherwise oxidize the Ni surface.[51,52]

Although water is by far the major component of all the solutions considered herein, the role played by dissolved species is further highlighted by our observation that adding small amounts of CH_3OH to alkali hydroxide solutions results in reduction of the Cu electrodes during x-ray illumination, rather than oxidation. CH_3OH is known to be a scavenger for $^{\bullet}OH$ radicals[53,54] which likely contributes to suppressing the Cu oxidation induced by the products of water radiolysis. Furthermore, the major products of CH_3OH radiolysis include H_2, CH_2O, CH_4, and CO,[55–57] which have standard electrode potentials significantly below those of the relevant Cu oxides, $E^0(CO_2/CO) = -0.104$ V,[48] $E^0(HCHO_2/CH_2O) = -0.029$ V,[48] $E_0(H^+/H_2) = 0.000$ V,[48] $E^0(CO_2/CH_4) = 0.169$ V,[48] and are thus thermodynamically capable of initiating Cu reduction. Again, these electrode potentials should be adjusted by -0.0592 V/pH as the pH is varied and thus the relative differences do not change. The shift from Cu oxidation towards reduction is therefore attributable to the generation of these products by CH_3OH radiolysis along with the scavenging of some of the oxidizing products of water radiolysis by CH_3OH.

Having rationalized a number of different ways in which x-ray induced radiolysis can influence the systems under investigation with operando x-ray spectroscopies, we now discuss several of the approaches that may be taken to mitigate the effects of radiolysis. This is also particularly relevant to attempts to use graphene membranes as electron-transparent membranes for XPS,[7–9] as the production of oxidizing radicals which can attack the graphene may negatively affect their stability during measurement.[4,15]

Perhaps the most obvious way to limit radiolysis is to reduce the number of photons impinging on the measured region. In many of the endstations used for soft-XAS, as much as 90% of the x-ray exposure time is associated with adjusting and stabilizing motors and other mechanical parts as the x-ray energy is scanned.[58] Implementing continuous scanning of the monochromator, and undulator (if used), with on-the-fly data collection can significantly reduce this "dead time" and thus minimize the required x-ray exposure during measurement.[58–61] Although this may come at the cost of energy resolution, this is likely to be an acceptable compromise in many atmospheric pressure measurement situations where avoiding changes to the chemistry of the system being studied is often more critical than obtaining ultimate resolution.

Further reducing the x-ray exposure, beyond eliminating the "dead time", will decrease the magnitude of the detectable spectroscopic signal and is therefore only feasible up to a point. Nonetheless, reducing the x-ray flux whilst simultaneously increasing the accumulation time to compensate, would provide additional time for reactive species to diffuse away and thus avoid their accumulation at the illuminated interface. This removal of reactive species generated by radiolysis may be further enhanced by continuously flowing a liquid/gas through the cell to rapidly replenish the reaction environment during measurement. Alternatively, the area from which the signal is obtained could be increased, allowing a lower x-ray flux per unit area whilst still obtaining a sufficiently large signal. This may be achieved by using less focused x-ray beams, or by scanning the sample relative to the beam so that the time-averaged x-ray flux per unit area is reduced. In either case, a corresponding increase in the size of the membrane region is required, whose maximum size will ultimately be limited by its structural stability and the pressure difference it must support (typically ~1 bar). For the case of scanning the sample, a further issue arises when performing TEY measurements as a transient photocurrent will be

generated on moving between regions which, unless it is sufficiently small or can be filtered out, may swamp the signal of interest.

Another promising approach is the use of scavenger species that react with or provide decay routes for the unwanted products of radiolysis, and we have observed here the important role that these can play in mitigating radiolysis effects. These may be dissolved or suspended in a solution, or placed in close proximity to the interface being probed.[62] Particular care is needed in selecting suitable scavengers for the system being studied to avoid altering the chemistry that we wish to probe. Indeed, as we have seen with CH_3OH, these scavengers may not just simply suppress the effects of radiolysis but through their own breakdown can completely change the interface chemistry.

A further method that may be considered is the use of electrical biasing to repel certain reactive species from the interface. We note however that this would only be effective against charged species of a certain polarity and it is unlikely to be feasible when investigating electrochemical environments as control over the biasing is needed to stimulate the reaction under investigation.

CONCLUSIONS

We have shown that under the conditions at which atmospheric pressure x-ray spectroscopies are performed, the effects of radiolysis at the interface between a solid electrode and a high-pressure gas or liquid environment can be significant. X-ray illumination leads to the generation of reactive species by radiolysis which can strongly influence the behavior observed in these systems. This is found to depend not only on the electrode material under consideration but also critically on the environment in which it is being measured. In air, and aqueous hydroxide

solutions, the predominantly oxidizing products of radiolysis lead to oxidation of Cu electrodes towards CuO. The addition of only small amounts of CH_3OH to the aqueous hydroxide solutions changes the balance of radiolysis products towards reducing species that cause the reduction of the electrode towards metallic Cu. We therefore emphasize that careful consideration of radiolysis effects is critical for drawing reliable conclusions from operando x-ray spectroscopy measurements, and highlight some promising approaches to mitigate the effects of radiolysis including the use of radical scavengers. The understanding developed by explicitly studying radiation effects is highly relevant to the application of x-ray characterization techniques at pressures and x-ray energies where radiolysis becomes significant.
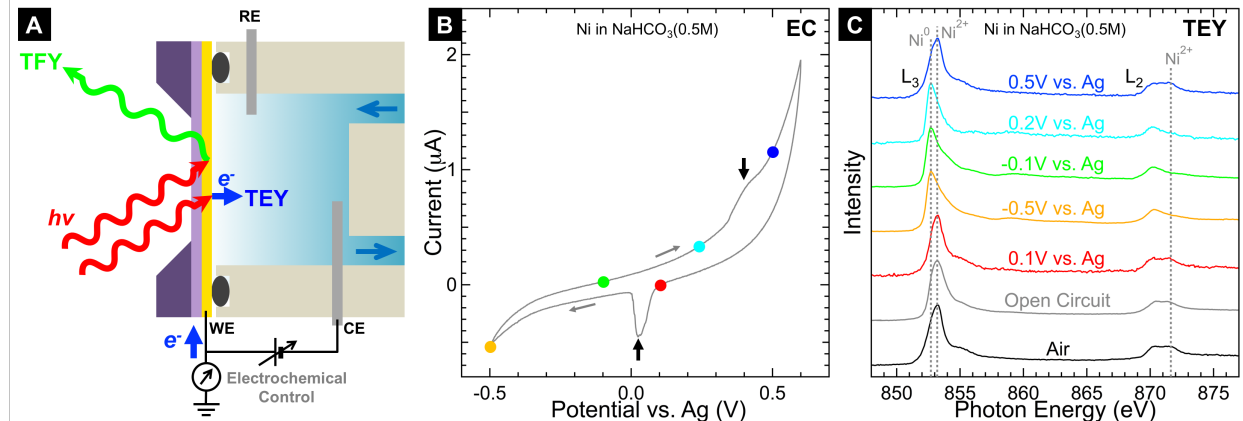
FIGURES

Figure 1. A) Cross-sectional schematic of electrochemical cell for in situ X-ray Absorption Spectroscopy (XAS), showing the liquid flow through the cell and the three-electrodes used to provide electrochemical control. A Si_3N_4(100 nm thick) membrane coated with a thin (~50 nm thick) metal film is used as working electrode [WE], a Ag wire as pseudo-reference electrode [RE], and a Pt wire as counter electrode [CE]. B) Cyclic voltammogram of Ni(50 nm) working electrode in an aqueous $NaHCO_3$ (0.5 M) solution, measured at a scan rate of 10 mV/s without x-ray illumination. Vertical black arrows indicate the peaks related to Ni reduction (~0.0 V) and oxidation (~0.4 V). C) Corresponding XAS of Ni $L_{2,3}$-edge measured with TEY mode in air at atmospheric pressure (black), and in an aqueous $NaHCO_3$ (0.5 M) solution under open circuit (grey) and while held at the potentials indicated by the colored dots in B. The acquisition time of each spectrum is ~1320s.
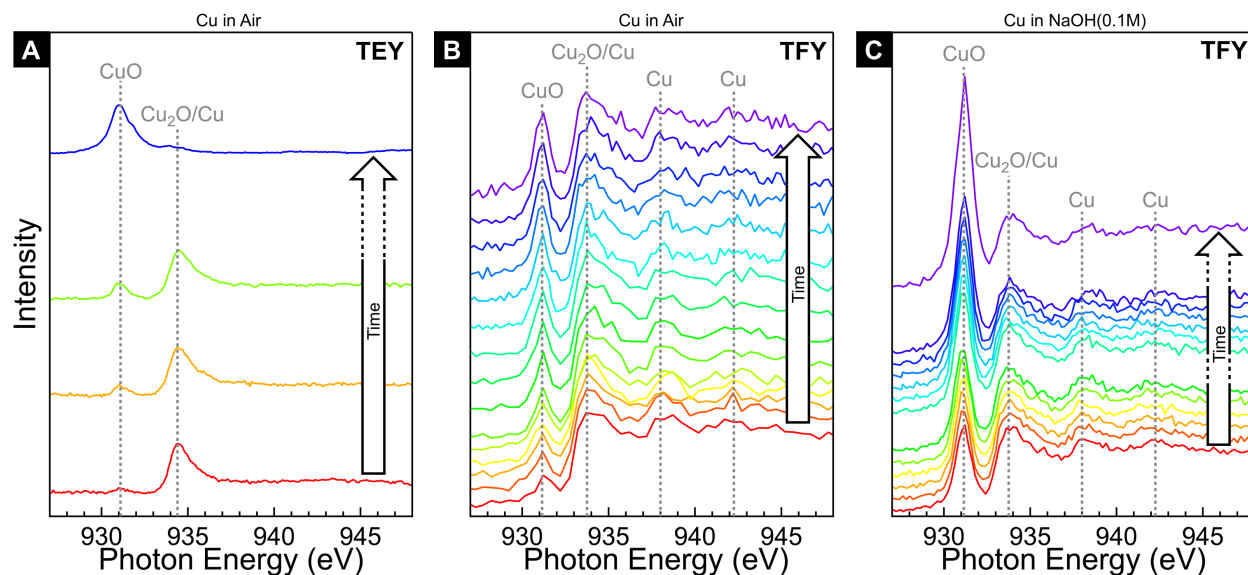
Figure 2: XAS of Cu L$_3$-edge for a Cu(50 nm) film in air and aqueous solutions. A) Measured in air at atmospheric pressure (1 bar) in TEY mode (interface sensitive) with each spectrum taking ~700s. The red, orange, and green spectra are started ~1400s apart, while the blue spectrum is measured after several hours of x-ray exposure. B) Measured in air at atmospheric pressure (1 bar) in TFY mode (bulk sensitive), with acquisition of the first six spectra started ~150s apart (red to green), and the remaining spectra started ~300s apart (green to violet). C) Measured in TFY mode after replacing the air by a 0.1 M aqueous solution of NaOH, with ~400s between the start of each spectrum acquisition, except for ~1300s between the sixth and seventh spectra, and ~2200s between the penultimate and final spectra.
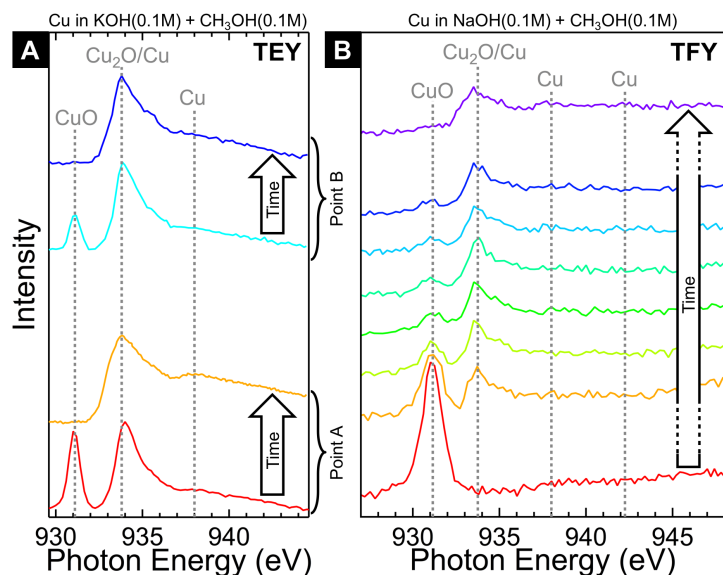
Figure 3: XAS of Cu L_3-edge for a Cu(50 nm) film measured in CH_3OH containing aqueous solutions. A) Measured in an aqueous solution of KOH(0.1 M) and CH_3OH(0.1 M) in TEY mode (interface sensitive), with each spectrum taking ~270s to acquire. There is an additional ~300s of x-ray exposure between the end of the red spectrum and start of the orange spectrum, whilst the blue spectrum is measured immediately after the cyan spectrum. B) Measured in an aqueous solution of NaOH(0.1 M) and CH_3OH(0.1 M) in TFY mode (bulk sensitive), with ~360s between the start of each spectrum acquisition, except for ~3600s between the first and second spectra, and ~2700s between the penultimate and final spectra.

AUTHOR INFORMATION

Corresponding Author

*rsw31@cam.ac.uk

ASSOCIATED CONTENT

Supporting Information

O K-edge spectra measured at corresponding conditions to the Ni $L_{2,3}$-edge spectra of Figure 1C.

REFERENCES

(1)   Schlögl, R. Heterogeneous Catalysis. *Angew. Chemie* **2015**, *54*, 3465–3520.

(2)   Goodenough, J. B. Electrochemical Energy Storage in a Sustainable Modern Society. *Energy Environ. Sci.* **2014**, *7*, 14–18.

(3)   Dunn, B.; Kamath, H.; Tarascon, J. Electrical Energy Storage for the Grid : A Battery of Choices. **2011**, *334*, 928–936.

(4)   Wu, C. H.; Weatherup, R. S.; Salmeron, M. B. Probing Electrode/electrolyte Interfaces in Situ by X-Ray Spectroscopies: Old Methods, New Tricks. *Phys. Chem. Chem. Phys.* **2015**, *17*, 30229–30239.

(5)   Escudero, C.; Salmeron, M. From Solid–vacuum to Solid–gas and Solid–liquid Interfaces: In Situ Studies of Structure and Dynamics under Relevant Conditions. *Surf. Sci.* **2013**, *607*, 2–9.

(6)   Jiang, P.; Chen, J.-L.; Borondics, F.; Glans, P.-A.; West, M. W.; Chang, C.-L.; Salmeron, M.; Guo, J. In Situ Soft X-Ray Absorption Spectroscopy Investigation of Electrochemical Corrosion of Copper in Aqueous NaHCO3 Solution. *Electrochem. commun.* **2010**, *12*, 820–822.

(7)   Kolmakov, A.; Dikin, D. A.; Cote, L. J.; Huang, J.; Abyaneh, M. K.; Amati, M.; Gregoratti, L.; Günther, S.; Kiskinova, M. Graphene Oxide Windows for in Situ Environmental Cell Photoelectron Spectroscopy. *Nat. Nanotechnol.* **2011**, *6*, 651–657.

(8)   Velasco-Velez, J. J.; Pfeifer, V.; Hävecker, M.; Weatherup, R. S.; Arrigo, R.; Chuang, C.-

H.; Stotz, E.; Weinberg, G.; Salmeron, M.; Schlögl, R.; *et al.* Photoelectron Spectroscopy at the Graphene-Liquid Interface Reveals the Electronic Structure of an Electrodeposited Cobalt/Graphene Electrocatalyst. *Angew. Chemie Int. Ed.* **2015**, *54*, 14554–14558.

(9)   Weatherup, R. S.; Eren, B.; Hao, Y.; Bluhm, H.; Salmeron, M. B. Graphene Membranes for Atmospheric Pressure Photoelectron Spectroscopy. *J. Phys. Chem. Lett.* **2016**, *7*, 1622–1627.

(10)   Eberhardt, W.; Sham, T. K.; Carr, R.; Krummacher, S.; Strongin, M.; Weng, S. L.; Wesner, D. Site-Specific Fragmentation of Small Molecules Following Soft-X-Ray Excitation. *Phys. Rev. Lett.* **1983**, *50*, 1038–1041.

(11)   Nenner, I.; Morin, P. Electronic and Nuclear Relaxation of Core-Excited Molecules. In *VUV and Soft X-ray Photoionization*; Becker, U.; Shirley, D. A., Eds.; Plenum Press: New York, 1996; pp. 291–354.

(12)   Yeh, J. J.; Lindau, I. Atomic Subshell Photoionization Cross Sections and Asymmetry Parameters: $1 \leq Z \leq 103$. *At. Data Nucl. Data Tables* **1985**, *32*, 1–55.

(13)   Royall, C. P.; Thiel, B. L.; Donald, A. M. Radiation Damage of Water in Environmental Scanning Electron Microscopy. *J. Microsc.* **2001**, *204*, 185–195.

(14)   Egerton, R. F.; Li, P.; Malac, M. Radiation Damage in the TEM and SEM. *Micron* **2004**, *35*, 399–409.

(15)   Stoll, J. D.; Kolmakov, A. Electron Transparent Graphene Windows for Environmental Scanning Electron Microscopy in Liquids and Dense Gases. *Nanotechnology* **2012**, *23*,

505704.

(16)   Schneider, N. M.; Norton, M. M.; Mendel, B. J.; Grogan, J. M.; Ross, F. M.; Bau, H. H.
         Electron-Water Interactions and Implications for Liquid Cell Electron Microscopy. *J.
         Phys. Chem. C* **2014**, *118*, 22373–22382.

(17)   Grogan, J. M.; Schneider, N. M.; Ross, F. M.; Bau, H. H. Bubble and Pattern Formation in
         Liquid Induced by an Electron Beam. *Nano Lett* **2014**, *14*, 0–5.

(18)   Ketteler, G.; Ashby, P.; Mun, B. S.; Ratera, I.; Bluhm, H.; Kasemo, B.; Salmeron, M. In
         Situ Photoelectron Spectroscopy Study of Water Adsorption on Model Biomaterial
         Surfaces. *J. Phys. Condens. MATTER* **2008**, *20*, 184024.

(19)   Jiang, P.; Porsgaard, S.; Borondics, F.; Köber, M.; Caballero, A.; Bluhm, H.;
         Besenbacher, F.; Salmeron, M. Room-Temperature Reaction of Oxygen with Gold : An In
         Situ Ambient-Pressure X-Ray Photoelectron Spectroscopy Investigation. *J. Am. Chem.
         Soc.* **2010**, *132*, 2858–2859.

(20)   Kraus, J.; Reichelt, R.; Günther, S.; Gregoratti, L.; Amati, M.; Kiskinova, M.; Yulaev, A.;
         Vlassiouk, I.; Kolmakov, A. Photoelectron Spectroscopy of Wet and Gaseous Samples
         through Graphene Membranes. *Nanoscale* **2014**, *6*, 14394–14403.

(21)   Pérez-Dieste, V.; Aballe, L.; Ferrer, S.; Nicolàs, J.; Escudero, C.; Milán, A.; Pellegrin, E.
         Near Ambient Pressure XPS at ALBA. *J. Phys. Conf. Ser.* **2013**, *425*, 72023.

(22)   Velasco-Velez, J.-J.; Wu, C. H.; Pascal, T. A.; Wan, L. F.; Guo, J.; Prendergast, D.;
         Salmeron, M. The Structure of Interfacial Water on Gold Electrodes Studied by X-Ray

Absorption Spectroscopy. *Science* **2014**, *346*, 831–834.

(23)   Pourbaix, M. *Lectures on Electrochemcial Corrosion*; Plenum Press: New York, 1973.

(24)   Regan, T. J.; Ohldag, H.; Stamm, C.; Nolting, F.; Lüning, J.; Stöhr, J.; White, R. L.

          Chemical Effects at Metal/oxide Interfaces Studied by X-Ray-Absorption Spectroscopy.

          Phys. Rev. B **2001**, *64*, 214422.

(25)   Weatherup, R. S.; D'Arsié, L.; Cabrero-Vilatela, A.; Caneva, S.; Blume, R.; Robertson, J.;

          Schlögl, R.; Hofmann, S. Long-Term Passivation of Strongly Interacting Metals with

          Single-Layer Graphene. *J. Am. Chem. Soc.* **2015**, *137*, 14358–14366.

(26)   Holloway, P. H.; Hudson, J. B. Kinetics of the Reaction of Oxygen with Clean Nickel

          Single Crystal Surfaces I - Ni(100) Surface. *Surf. Sci.* **1974**, *43*, 141–149.

(27)   Lambers, E. S.; Dykstal, C. N.; Seo, J. M.; Rowe, J. E.; Holloway, P. H. Room-

          Temperature Oxidation of Ni(110) at Low and Atmospheric Oxygen Pressures. *Oxid. Met.*

          1996, *45*, 301–321.

(28)   Seghiouer, A.; Chevalet, J.; Barhoun, A.; Lantelme, F. Electrochemical Oxidation of

          Nickel in Alkaline Solutions: A Voltammetric Study and Modelling. *J. Electroanal.*

          Chem. **1998**, *442*, 113–123.

(29)   Wang, D.; Zhou, J.; Hu, Y.; Yang, J.; Han, N.; Li, Y.; Sham, T.-K. In Situ X-Ray

          Absorption Near-Edge Structure Study of Advanced NiFe(OH) X Electrocatalyst on

          Carbon Paper for Water Oxidation. *J. Phys. Chem. C* **2015**, *119*, 19573–19583.

(30)   Visscher, W.; Barendrecht, E. The Anodic Oxidation of Nickel in Alkaline Solution.

Electrochim. Acta **1980**, *25*, 651–655.

(31)   Paik, W.; Szklarska-Smialowska, Z. Reflectance and Ellipsometric Study of Anodic Passive Films Formed on Nickel in Sodium Hydroxide Solution. *Surf. Sci.* **1980**, *96*, 401–412.

(32)   Smith, R. J.; Hummel, R. E.; Ambrose, J. R. The Passivation If Nickel in Aqueous Solutions-II. An in Situ Investigation of the Passivation of Nickel Using Optical and Electrochemical Techniques. *Corr. Sci.* **1987**, *27*, 815–826.

(33)   Hummel, R. E.; Smith, R. J.; Verink, E. D. The Passivation of Nickel in Aqueous Solutions-I. The Identification of Insoluble Corrosion Products on Nickel Electrodes Using Optical and ESCA Techniques. *Corros. Sci.* **1987**, *27*, 803–813.

(34)   Tanuma, S.; Powell, C. J.; Penn, D. R. Calculations of Electron Inelastic Mean Free Paths. IX. Data for 41 Elemental Solids over the 50 eV to 30 keV Range. *Surf. Interface Anal.* **2011**, *43*, 689–713.

(35)   X-Ray Attenuation Length http://henke.lbl.gov/cgi-bin/atten.pl (accessed Jun 9, 2017).

(36)   Willis, C.; Boyd, A. W.; Young, M. J. Radiolysis of Air and Nitrogen–Oxygen Mixtures with Intense Electron Pulses: Determination of a Mechanism by Comparison of Measured and Computed Yields. *Can. J. Chem.* **1970**, *48*, 1515–1525.

(37)   Eren, B.; Heine, C.; Bluhm, H.; Somorjai, G. A.; Salmeron, M. Catalyst Chemical State during CO Oxidation Reaction on Cu(111) Studied with Ambient-Pressure X-Ray Photoelectron Spectroscopy and Near Edge X-Ray Adsorption Fine Structure

Spectroscopy. *J. Am. Chem. Soc.* **2015**, *137*, 11186–11190.

(38)   Eren, B.; Weatherup, R. S.; Liakakos, N.; Somorjai, G. A.; Salmeron, M. B. Dissociative

Carbon Dioxide Adsorption and Morphological Changes on Cu(100) and Cu(111) at

Ambient Pressures. *J. Am. Chem. Soc.* **2016**, *138*, 8207–8211.

(39)   van Elp, J.; Searle, B. G.; Sawatzky, G. A.; Sacchi, M. Ligand Hole Induced Symmetry

Mixing of d8 States in LixNi1-xO, as Observed in Ni 2p X-Ray Absorption Spectroscopy.

Solid State Commun. **1991**, *80*, 67–71.

(40)   van Veenendaal, M. A.; Sawatzky, G. A. Doping Dependence of Ni 2p X-Ray-Absorption

Spectra of MxNi1-xO(M =Li,Na). *Phys. Rev. B* **1994**, *50*, 11326–11331.

(41)   Mossanek, R. J. O.; Domínguez-Cañizares, G.; Gutiérrez, A.; Abbate, M.; Díaz-

Fernández, D.; Soriano, L. Effects of Ni Vacancies and Crystallite Size on the O 1s and Ni

2p X-Ray Absorption Spectra of Nanocrystalline NiO. *J. Phys. Condens. Matter* **2013**, *25*,

495506.

(42)   Holloway, P. H. Chemisorption and Oxide Formation on Metals: Oxygen–nickel

Reaction. *J. Vac. Sci. Technol.* **1981**, *18*, 653–659.

(43)   Hill, M. A.; Smith, F. A. Calculation of Initial and Primary Yields in the Radiolysis of

Water. *Radiat. Phys. Chem.* **1994**, *43*, 265–280.

(44)   Draganic, Z. D.; Draganic, I. G. Formation of Primary Yields of Hydroxyl Radical and

Hydrated Electron in the .gamma.-Radiolysis of Water. *J. Phys. Chem.* **1973**, *77*, 765–

772.

(45)   Draganić, Z. D.; Draganić, I. G. On the Origin of Primary Hydrogen Peroxide Yield in the

          Gamma Radiolysis of Water. *J Phys Chem* **1969**, *73*, 2571–2577.

(46)   Schwarz, H. A. Free Radicals Generated by Radiolysis of Aqueous Solutions. *J. Chem.*

          Educ. **1981**, *58*, 101–105.

(47)   Vanýsek, P.; Elec-, V. K. T. S. Electrochemical Series. *CRC Handb. Chem. Physics, 97th*

          Ed. Sect. 5 Thermo, Electro Solut. Chem. **2016**, 5-78-84.

(48)   Bratsch, S. G. Standard Electrode Potentials and Temperature Coefficients in Water at

          298.15 K. *J. Phys. Chem. Ref. Data* **1989**, *18*, 1–21.

(49)   Koppenol, W. H.; Liebman, J. F. The Oxidizing Nature of the Hydroxyl Radical. A

          Comparison with the Ferryl Ion (FeO2+). *J. Phys. Chem.* **1984**, *88*, 99–101.

(50)   Armstrong, D. A.; Huie, R. E.; Koppenol, W. H.; Lymar, S. V.; Merenyi, G.; Neta, P.;

          Ruscic, B.; Stanbury, D. M.; Steenken, S.; Wardman, P. Standard Electrode Potentials

          Involving Radicals in Aqueous Solution: Inorganic Radicals (IUPAC Technical Report).

          Pure Appl. Chem. **2015**, *87*, 1139–1150.

(51)   Haygarth, K. S.; Marin, T. W.; Janik, I.; Kanjana, K.; Stanisky, C. M.; Bartels, D. M.

          Carbonate Radical Formation in Radiolysis of Sodium Carbonate and Bicarbonate

          Solutions up to 250 °C and the Mechanism of Its Second Order Decay. *J. Phys. Chem. A*

          2010, *114*, 2142–2150.

(52)   Balachandran, R.; Zhao, M.; Dong, B.; Brown, I.; Raghavan, S.; Keswani, M. Role of

          Ammonia and Carbonates in Scavenging Hydroxyl Radicals Generated during Megasonic

Irradiation of Wafer Cleaning Solutions. *Microelectron. Eng.* **2014**, *130*, 82–86.

(53)   Monod, A.; Chebbi, A.; Durand-Jolibois, R.; Carlier, P. Oxidation of Methanol by

Hydroxyl Radicals in Aqueous Solution under Simulated Cloud Droplet Conditions.

Atmos. Environ. **2000**, *34*, 5283–5294.

(54)   Dorfman, L. M.; Adams, G. E. Reactivity of the Hydroxyl Radical in Aqueous Solutions.

NSRDS-NBS **1973**, *46*, 1–72.

(55)   Baxendale, J. H.; Mellows, F. W. The γ-Radiolysis of Methanol and Methanol Solutions.

J. Am. Chem. Soc. **1961**, *83*, 4720–4726.

(56)   Baxendale, J. H.; Wardman, P. The Radiolysis of Methanol: Product Yields, Rate

Constants, and Spectroscopic Parameters of Intermediates. *NSRDS-NBS* **1975**, *54*, 1–26.

(57)   Chen, Y.-J.; Ciaravella, A.; Muñoz Caro, G. M.; Cecchi-Pestellini, C.; Jiménez-Escobar,

A.; Juang, K.-J.; Yih, T.-S. Soft X-Ray Irradiation of Methanol Ice: Formation of Products

As a Function of Photon Energy. *Astrophys. J.* **2013**, *778*, 162.

(58)   Joly, L.; Otero, E.; Choueikani, F.; Marteau, F.; Chapuis, L.; Ohresser, P. Fast Continuous

Energy Scan with Dynamic Coupling of the Monochromator and Undulator at the

DEIMOS Beamline. *J. Synchrotron Radiat.* **2014**, *21*, 502–506.

(59)   Frahm, R. Quick Scanning Exafs: First Experiments. *Nucl. Inst. Methods Phys. Res. A*

1988, *270*, 578–581.

(60)   Frahm, R. New Method for Time Dependent X-Ray Absorption Studies. *Rev. Sci. Instrum.*

1989, *60*, 2515–2518.

(61)   Solé, V. A.; Gauthier, C.; Goulon, J.; Natali, F. Undulator QEXAFS at the ESRF

Beamline ID26. *J. Synchrotron Radiat.* **1999**, *6*, 174–175.

(62)   Cho, H.; Jones, M. R.; Nguyen, S. C.; Hauwiller, M. R.; Zettl, A.; Alivisatos, A. P. The

Use of Graphene and Its Derivatives for Liquid-Phase Transmission Electron Microscopy

of Radiation-Sensitive Specimens. *Nano Lett.* **2017**, *17*, 414–420.

TOC Graphic